NEW MONOCRYSTALS WITH LOW PHONON ENERGY FOR MID-IR LASERS

New Monocrystals

LUDMILA ISAENKO, ALEXANDER YELISSEYEV
Institute of Geology & Mineralogy, Russian Academy of Sciences, Siberian branch, 3, ac. Koptyug avenue, Novosibirsk 630090 Russian Federation

ALEXANDRA TKACHUK*, SVETLANA IVANOVA
S.I. Vavilov State Optical Institute, 12, Birzhevaja line, St. Petersburg 199034 Russian Federation

Abstract. Various aspects of crystal growth, structure, physical and optical properties of new low phonon energy crystals, namely the rare earth doped alkali-lead halide crystals RE^{3+}: MPb_2Hal_5($M = Rb, K$ and $Hal = Cl, Br$), are described. The crystals were grown using the Bridgman technique, most of crystals were grown for the first time. The results of spectroscopic study of the RE^{3+}-doped double chloride crystals, RE^{3+}:KPb_2Cl_5 ($RE^{3+} = Pr^{3+}, Nd^{3+}, Tb^{3+}$, $Dy^{3+}, Ho^{3+}, Er^{3+}, Yb^{3+}$), and new double bromide KPb_2Br_5 and $RbPb_2Br_5$ crystals doped with Nd^{3+} and Tb^{3+} are presented, including multiphonon non-radiative relaxation rates, and absorption and emission spectra. Judd-Ofelt intensity parameters, as well as radiative transition probabilities, lifetimes, and branching ratios are summarized. The efficiency of up-conversion is demonstrated in Nd and Er doped KPb_2Cl_5 crystals. The luminescence dynamics and energy transfer processes responsible for population of excited RE^{3+} levels and laser action are discussed. The possibility of laser action in the mid-infrared is considered.

Keywords: Double alkali-lead halides, crystal growth, phase transitions, crystal structure, optical properties, rare earth ions, optical spectra, phonon spectrum, absorption cross section, energy transfer, upconversion, multiphonon relaxation, population dynamics, laser action.

1. Introduction

Mid-infrared (mid-IR) solid state lasers operating in the 3–10 μm spectral range are of great importance because of the overwhelming variety of fundamental and practical applications such as next-generation imaging devices, near-IR quantum

* Alexandra Tkachuk, P.O. box 37, St. Petersburg 195197, RUSSIA. Fax +7(812)328 58 91; e-mail: tkachuk@mail.rcom.ru

M. Ebrahim-Zadeh and I. T. Sorokina (eds.), Mid-Infrared Coherent Sources and Applications, 3–65.

counting devices, remote sensing, molecular and solid state spectroscopy, clinical and diagnostic analysis, atmospheric sensing, optical metrology, and medicine.

Currently, optical parametric oscillator systems are typically used to cover these wavelengths. These systems incorporate both nonlinear media and pump laser sources, leading to some complexity of the optical system.

Another simpler approach to solve these problems is direct mid-IR laser operation in solid-state media. In this case, direct pumping of the working laser level is of specific interest for the development of mid-IR lasers with high efficiency. To achieve an acceptable quantum efficiency from a given energy level it is necessary to avoid luminescence quenching via multiphonon relaxation depending on energy gap and maximal phonon energy in given host material. Therefore, the host material must have low phonon frequency, which will ensure low non-radiative losses. Multiphonon quenching of closely-spaced energy levels limits laser operation to wavelengths near and shorter than 3 μm in host-matrices based on the oxygen-containing compounds (e.g. YAG, YSGG, GGG, $YAlO_3$, YVO_4, $CaWO_4$) doped with Rare Earth (RE) ions [1].

More success has been achieved with laser operation in the range shorter than 4 μm with rare-earth-doped fluoride hosts, having effective phonon frequency of 400–560 cm^{-1}, about two times lower then in the oxygen containing compounds.

Under direct pumping, laser action with double fluoride crystals has been achieved at 2.8–2.9 μm on Er^{3+} laser transition $^4I_{11/2} \rightarrow {}^4I_{13/2}$ in $LiYF_4$ [2–15], BaY_2F_8 [16–19], $Na_{0.4}Y_{0.6}F_{2.2}$ [20], on Ho^{3+} laser transition $^5I_6 \rightarrow {}^5I_7$ in $BaYb_2F_8$ [21, 22], $LiYbF_4$ [23], and at 3.0–3.4 μm on Dy^{3+} laser transition $^6H_{13/2} \rightarrow {}^6H_{15/2}$ in $Ba(Y, Yb)_2F_8$ [24, 25] and LaF_3 [26]. Laser action at 3.4–4.4 μm has been achieved on Dy^{3+} laser transition $^6H_{11/2} \rightarrow {}^6H_{13/2}$ in YLF [27]; on Ho^{3+} laser transitions $^5S_2 \rightarrow {}^5F_5$ [28] and $^5I_5 \rightarrow {}^5I_6$ [29] in $LiYF_4$, and on Pr^{3+} laser transition $^1G_4 \rightarrow {}^3F_4$ in $BaYb_2F_8$ [30].

Currently, the RE-doped sulfide and chloride hosts attract particular attention due to the possibility of laser action beyond the 4-μm limit owing to their lower vibrational frequencies and higher quantum yields. These low phonon energy hosts have extremely low non-radiative rates and have been demonstrated to be very advantageous for direct diode-pumped solid-state lasers operating in the 3–9 μm region [31–40]. Room temperature laser action in Dy^{3+}-doped $CaGa_2S_4$ crystal at 4.31 μm was first reported in [37]. Tunable room-temperature laser action near 4.3–4.4 μm has been demonstrated in low-phonon-energy nonhygroscopic sulfide host (calcium thiogallate $CaGa_2S_4$) doped with Dy^{3+}, and it was noted that the 4.3 μm laser emission is in accordance with the five-times-maximal phonon energy rule of thumb, suggesting that laser emission up to 5.7 μm is possible. Some advantages in output laser efficiency of Dy^{3+}-doped lead thiogallate ($PbGa_2S_4$:Dy^{3+}) over $CaGa_2S_4$ was demonstrated in [41].

The longest laser wavelength of 7.2 μm has been achieved with the low-phonon-energy host lanthanum trichloride ($LaCl_3$) doped with Pr^{3+} [42].

However, Pr:$LaCl_3$ crystal has the disadvantage of being highly hygroscopic and lasing at low temperatures ($T < 200\,K$).

An important step towards practicality was made when the rare-earth-doped alkali-lead halide crystals MPb_2Hal_5 (M = Rb, K and Hal = Cl, Br) were identified as promising new low-phonon-energy host materials for mid-IR applications.

First, potassium-lead double chloride crystals KPb_2Cl_5 (KPC) were synthesized and studied in 1993 [43]. They show high chemical resistance, satisfactory mechanical properties, and have low hygroscopicity, unlike the known simple tri-chloride crystals (RE:$LnCl_3$).

The KPC material was assigned a promising new laser host material for rare-earth ion doping, and having narrow phonon spectrum ($\hbar\omega_0 \sim 203\,cm^{-1}$) [44]. The KPC crystal was found to exhibit superior spectroscopic and mechanical properties desirable for practical solid-state mid-IR lasers.

Direct pump laser action in Er^{3+}:KPC at both 1.7 and 4.5 μm from the erbium $^4I_{9/2}$ manifold has been demonstrated [45]. In Nd^{3+}:KPC, laser operation was obtained on the $^4F_{3/2} \rightarrow {}^4I_{11/2}$ transition at 1.06 μm with a slope efficiency of 7.7 % [38] and in Dy^{3+}:KPC laser action was demonstrated on the $(^6H_{9/2} + {}^6F_{11/2}) \rightarrow {}^6H_{13/2}$ transition at 2.43 μm [37]. New IR emission in Dy-doped KPC single crystals around 1.55 μm on the promising $^6F_{5/2} \rightarrow {}^6H_{11/2}$ laser transition is also reported [46].

Narrower phonon spectra are exhibited by bromide crystals. The alkali-lead bromide crystals ($RbPb_2Br_5$ and $CsPbBr_3$) were grown first in 1995 and the results of the study of crystal growth and luminescence properties were reported [47]. An efficient purification procedure of starting bromides was proposed and single crystals without cracks, 20 mm in diameter and 30–50 mm in length, have been prepared. Luminescence of undoped $RbPb_2Br_5$ crystal was measured for the first time [47].

The rare-earth-doped potassium-lead bromide (KPb_2Br_5 or KPB) and rubidium-lead bromide ($RbPb_2Br_5$ or RPB) crystals have properties similar to that of KPC crystals, but lower phonon cut-off energy ($\sim 140\,cm^{-1}$) [48]. They may be considered as the best matrix for minimizing the primary cause of the passive losses in laser rod arising from nonradiative multiphonon relaxation, therefore, these hosts permit lasing at longer wavelengths with extremely low thermal losses. Laser action in near-IR was demonstrated in Nd^{3+}-doped KPB and RPB crystals [48]. Spectroscopic study of the Tb^{3+}:KPB crystals gave evidence that room-temperature laser action should be possible in the mid-IR up to 9 μm [48].

Thus, the rare-earth-doped potassium- and rubidium-lead double halogenides MPb_2Hal_5 (M = K, Rb; Hal = Cl, Br) can be considered as promising new materials emitting in a wide spectral range from the UV to mid IR. Interest in these crystals continues to increase each year. Having low hygroscopicity, high chemical resistance, good mechanical properties, and low maximal-phonon

frequency, they are readily manufactured and available in a large size of high optical quality for applications in solid-state lasers.

The low phonon frequency of chloride and bromide crystals allows rare-earth ions to serve as favorable luminescent centers for laser action over a wide range in the IR and UV-visible spectral regions, where the luminescence of fluoride and oxide crystals is quenched by fast multiphonon relaxation.

In the present work we considered the crystal growth, physical and optical properties of new laser crystals based on RE^{3+}-doped alkali-lead halide matrices, which are suitable for diode-pumped IR, visible and UV lasers. The RE^{3+}-doped double chloride crystals, RE^{3+}:KPb_2Cl_5(RE^{3+} = Pr^{3+}, Nd^{3+}, Tb^{3+}, Dy^{3+}, Ho^{3+}, Er^{3+}, Tm^{3+}, Yb^{3+}), and new double bromides KPb_2Br_5 and $RbPb_2Br_5$ doped with Nd^{3+} and Tb^{3+}, were grown using the Bridgman technique. Most crystals were grown for the first time. Multiphonon non-radiative relaxation rates were estimated for the studied hosts. The absorption and luminescence spectra, Judd-Ofelt intensity parameters, calculated radiative transition probabilities, lifetimes and branching ratios are summarized. The intense luminescent bands in the UV, visible, and near-IR spectral regions show that all excited levels of RE^{3+} ions separated by energy gap of $\Delta E > 1400\,cm^{-1}$ in chlorides and of $\Delta E > 1000\,cm^{-1}$ in bromides are radiative, including $^4I_{9/2}$ (Er), $^5I_5$ (Ho), and $^4F_{5/2}$ (Nd) levels, which are considerably quenched in oxides and fluorides. The combination of the high intensity of luminescent transitions and long lifetime of rare-earth radiative levels, together with efficient up-conversion processes, permit us to conclude that MPb_2Hal_5:RE^{3+} crystals may be considered as promising new luminescent materials for UV, mid-IR, and visible laser-diode-pumped lasers.

2. Crystal growth and common properties of RE-doped MPb_2Hal_5 (M = K, Rb; Hal = Cl, Br) crystals

2.1. CRYSTAL GROWTH

Synthesis of MPb_2Hal_5 compounds with M = K, Rb, Hal = Cl, Br was performed from high purity chloride salts. The starting high purity (99.999%) reagents, $PbCl_5$, $PbBr_2$, KCl, KBr, RbCl and RbBr, were additionally purified by repeated directed crystallization by preliminarily removing of dirty parts. $REHal_3$ was synthesized from RE oxides, 99.99%, with further distillation. The MPb_2Hal_5 (M = K, Rb, Hal = Cl, Br) single crystals were grown using Bridgman technique in soldered ampoules with halogen atmosphere [32, 40, 43, 49–51]. To prevent compound decomposition, the internal ampoule pressure exceeded the atmospheric pressure. As follows from phase diagrams (*Figure* 1), KPC, KPB and RPB melt congruently at 434, 382 and 404° C, respectively [49, 52]. Linear temperature gradient in a growth zone of the furnace was $\sim 20\,^\circ$/cm and the rate

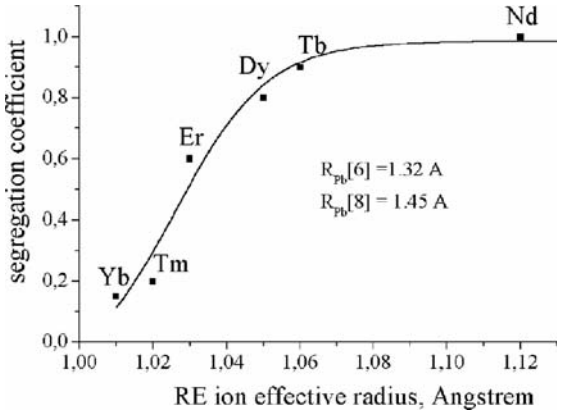

Figure 2. Segregation coefficients for RE ions in KPC. The Pb radii are given for cubic and octahedral coordination.

transitions are often a reason for twin structure formation and sharply worsen the optical quality of the crystal.

2.2. PHASE TRANSITIONS

Using a set of optical techniques such as differential scanning microcalorimetry, temperature dependence of birefringence and turning angle of optical indicatrix, the phase transitions were studied in MPb_2Hal_5 (M = K, Rb, Hal = Cl, Br) crystals in the 270 to 620 K temperature range [53, 54]. Depending on the ratios of ionic radii, M/Hal and Pb/Hal, these compounds can be related to two structural types: monoclinic $\mathbf{P2_1/c}$ and tetragonal $\mathbf{I4/mcm}$ [55]. Examinations showed phase transitions at 530 K/528 K in KPC and at 519.5/518.5 K in KPB in the heating/cooling regimes, respectively. The obtained data are in good agreement with previous data [52]. Phase transition is accompanied by a birefringence jump and a temperature hysteresis, which are typical of first type transitions. Geometry of twinning and turning of optical indicatrix shows that the phase is monoclinic with second-order axis along [010] at room temperature, which is in agreement with the $\mathbf{P2_1/c}$ symmetry. As follows from observations in polarized light a high temperature phase has rhombic symmetry. This phase transition is related to ferroelastic ones of first type, with $\Delta H = 1000 \pm 200$ J/mol and 1300 ± 200 J/mol enthalpy changes for KPC and KPB, respectively. The transition is accompanied by twinning and $\mathbf{mmm} \longleftrightarrow \mathbf{P2_1/c}$ symmetry changes. As a result of such transition, a component of shear spontaneous deformation appears and crystal is broken into twins with a $\pm\varphi$ turning around [010] for optical indicatrix. One can see in *Figure* 3 that temperature dependence $\varphi = \varphi(T)$ is very unusual for KPC: at room temperature φ angle is small (only $\sim$1 to 2° as follows from points 1). This value remains constant with heating and it increases to only 5° near phase transition, but

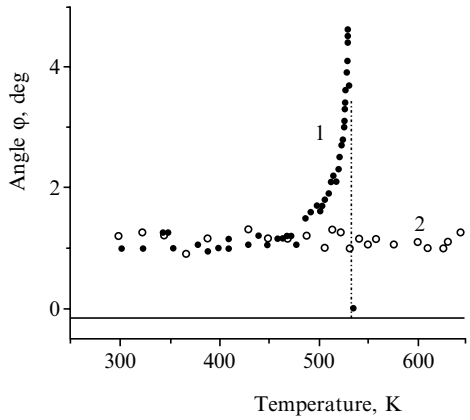

Figure 3. Temperature dependence for a turning angle of the optical indicatrix φ(T) for KPC (1) and RPC (2) [54].

falls to zero afterwards. With further heating, extinction in the sample does not change. For RPC (points 2 in *Figure* 3) a value of off-orientation angle between adjacent areas does not change up to the melting temperature. There is no phase transition here and as a result we see no twin structure. The same situation (no twins, no phase transitions) also takes place in RPB, which crystallizes in tetragonal structure. Thus change of halogen ion and passing from chlorides to bromides in an MPb_2Hal_5 family slightly decreases a boundary for rhombic phase stability, whereas a cation change with passing from potassium to rubidium increases this temperature, shifting the phase transition to the liquid state of the compound. Thus, RPB structure has tetragonal **I4/mcm** symmetry and this structure is stable up to the melting temperature.

2.3. STRUCTURAL ANALYSIS

Previously crystal structure of double chlorides was studied [56–58]. The single crystal structural analysis was carried out for all crystals of MPb_2Hal_5 family using a STOE STADI4 diffractometer with a Mo K_α radiation. The refined lattice parameters for MPb_2Hal_5 crystals are given in TABLE 1.

In MPb_2Hal_5 structure one can distinguish the layers from polyhedrons $KHal_9$ and $Pb(1)Hal_9$, bound together by joint triangular faces: these layers are alternating along direction perpendicular to x axis (*Figure* 4). The Pb(2) ions are in asymmetric anionic cavities (*Figure* 4). The K and Pb(1) polyhedrons are tri-cap trigonal prisms, whereas $Pb(2)Hal_8$ polyhedron is close to a tetragonal antiprism. Asymmetry in Pb(2) position in a Hal_6 cycle brings to an umbrella character of cations location in polyhedrons. Cavities for Pb in chloride matrix and even to a larger extent in bromide matrix are too large for a Pb^{2+} cation: as a result Pb ions are shifted outside cavity center in both positions and pressed to one of the

TABLE 1. Results of structural analysis for MPb_2Hal_5 [59].

Crystal	Symmetry	Lattice parameters, $\mathbf{Z} = \mathbf{4}$				
		$\boldsymbol{a}$(Å)	$\boldsymbol{b}$(Å)	$\boldsymbol{c}$(Å)	β, degrees	$\boldsymbol{V}$(Å^3)
KPb_2Cl_5	$P2_1/c$	8.854(2)	7.927(2)	12.485(3)	90.05(3)	876.3(4)
KPb_2Br_5	$P2_1/c$	9.256(2)	8.365(2)	13.025(3)	90.00(3)	1008.4(4)
$RbPb_2Cl_5$	$P2_1/c$	8.959(2)	7.973(2)	12.492(5)	90.12(2)	892.3(4)
$RbPb_2Br_5$	$I4/mcm$	8.43(1)	8.43(1)	14.54(1)	90	1033(4)

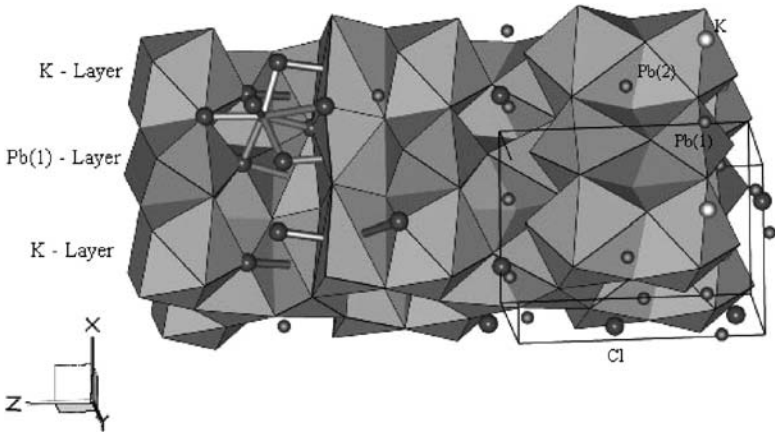

Figure 4. The KPB structure presented as combination of K and Pb(1) polyhedrons.

cavity walls. Imperfection of single crystal KPB samples depends strongly on a microtwin structure. Study of samples with different microtwinning brought one to the following conclusion: microtwinning results in increase of the sample volume and a decrease of monoclinic angle to 90°; in other words microtwinning results in pseudorhombic unit cell.

Optical measurements in polarized light showed that twin sizes are of about several microns, whereas the twinning pattern depends on thermal prehistory of the sample. In *Figure* 5 two KPC crystallographic unit cells are shown. One can see that YZ plane is close to a mirror plane. After twinning operation relative to the X (-x,y,z) axis, one obtains K′, Pb′ and Cl′ positions, which are close to positions of these atoms in the initial cells. Maximal distances between atom positions in the initial cell and in the twin cell are 0.11, 0.16, 0.64 and 1.03 Å for Pb(1)-Pb(1)′, K-K′, Cl(2)-Cl(2)′ and Pb(2)-Pb(2)′, respectively. For other Cl atoms these distances are less than 0.1 Å. Thus distances between atom positions of corresponding atoms in initial and twin cells are less than a half of the bond

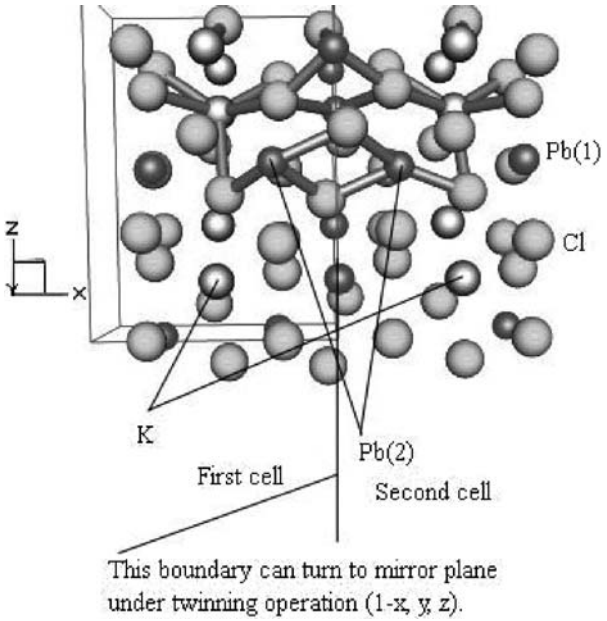

Figure 5. Superposition of two crystallographic unit cells in the KPC structure. One type of unit cell is shown at left from the central vertical line and the other one, obtained after twinning operation (1-x, y, z), is shown at right.

length. Maximal shift is observed for Pb(2), which corresponds to atom jump from one half of the elongated Cl_6 cycle in YZ plane to another half of the cycle. This allows one to suppose that twinning happens by hopping mechanism at crystal cooling and depends considerably on a set of point and extended defects, which are formed during crystal growth. The β angle is close to 90° for crystals under consideration, which promotes twinning relative to Y and Z axes. The RE ions incorporation into crystal lattice is supposed to go with Pb ions substitution, whereas formation of K vacancy provides local charge compensation.

2.4. OPTICAL PROPERTIES OF UNDOPED MPB_2HAL_5 CRYSTALS

Since low frequency crystal dynamics is important both from fundamental and applications point of view, the study of optical properties of new low phonon energy crystals included refractive indices with their dispersion curves and temperature dependence, Raman, absorption, reflection and emission spectra of undoped MPb_2Hal_5 crystals, including the nature of UV host absorption bands.

2.4.1. *Refractive indices and thermo-optic coefficients*

Refractive indices were measured using a conventional technique of minimum deviation angle with two prisms of different orientation: ***n*** values were found to

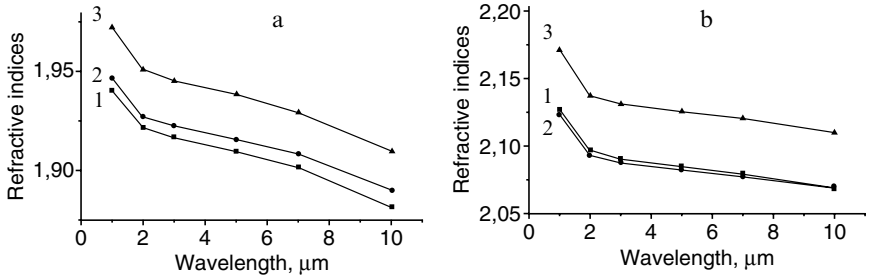

Figure 6. Refractive indices n_x (1), n_y (2) and n_z (3) versus wavelength in the 1 to 10 micron range for KPC (a) and KPB (b) at 300 K.

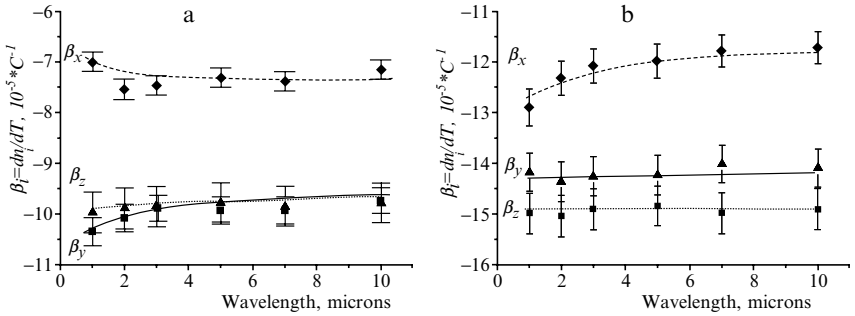

Figure 7. Thermooptic coefficients $\beta_i = dn_i/dT$ with i = x, y, z for KPC (a) and KPB (b).

grow in the set KPC → RPC → KPB → RPB. Dispersion characteristics for KPC and KPB are given in *Figure* 6. In accordance with lattice parameters, n_x and n_y values are close, whereas n_z values are considerably larger. Temperature dependence at 6 wavelengths (1, 2, 3, 5, 7 and 10 μm) was studied using a specially controlled heating device, which was mounted on the optical goniometer, and thermo-optic coefficients $\beta_i = dn_i/dT$ were calculated: they are given in *Figure* 7 for KPC and KPB. One can see that refractive indices n_i and β_i values become larger in bromides as ion sizes and lattice parameters increase and crystal lattice becomes more friable. These parameters are considerably anisotropic: β_x values are about 30 % higher than β_y, β_z.

2.4.2. *Vibrational (Raman) spectra*

Since low frequency crystal dynamics is important both from fundamental and applications point of view, the Raman spectra were studied. For interpretation of vibrational spectra and establishment of lattice vibration frequency-to-structure correlations, we used the recently developed first-principles approach [60–62]. It is necessary to note that empirical techniques traditionally used ([63, 64], for example) bring in a large number of adjusting parameters in the case of low symmetry structures with many atoms in the unit cell, and it is impossible to

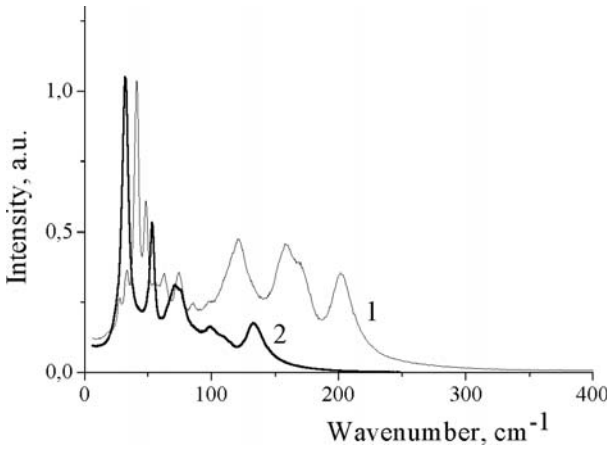

Figure 8. Raman spectra for KPC (1) and KPB (2) crystals.

determine these parameters using a limited amount of experimental data. Thus, the use of parameter-free techniques becomes fundamentally important.

Raman spectra were recorded in polarized light at room temperature for MPb_2Hal_5 samples with edges oriented along crystallographic axes. For KPb_2Cl_5 and KPb_2Br_5, the vibrational representation is reduced to the following irreducible representations in the center of Brillouin zone:

$$\Gamma = 24A_g(xx, yy, zz, xy, yx) + 24B_g(xz, zx, yz, zy) + 24A_u + 24B_u, \quad (1)$$

where the parentheses contain the Raman tensor components for which the corresponding lattice vibrations are active. The experimental spectra are shown in *Figure* 8. As expected, the spectra are restricted to frequencies $h\omega_{max} < 250\,cm^{-1}$ and $h\omega_{max} < 150\,cm^{-1}$, with high frequency peaks located at 203 and $138\,cm^{-1}$, respectively; the spectra are strongly anisotropic, and the spectral lines are highly polarized. The number of well-resolved peaks is slightly smaller than the number of modes determined from Eq. (1); therefore, their interpretation requires comparison of the peaks with the results of model calculations.

Taking these distortions into account is especially important for low-symmetry structures, since the interactions of multiple moments of ions in these structures contribute substantially to the total lattice energy and the crystal vibration frequency. The short-range part of inter-ionic interactions is calculated in terms of density functional theory, whereas for far-ranging part we used a multipole expansion (up to quadrupoles); multipole moments were found by minimizing the total crystal energy with respect to the corresponding moment.

The eigenvectors were obtained by diagonalizing the dynamical matrix and subjected to symmetry analysis. The complete vibrational representation P(g) of the crystal space group was constructed and it was used further to calculate the

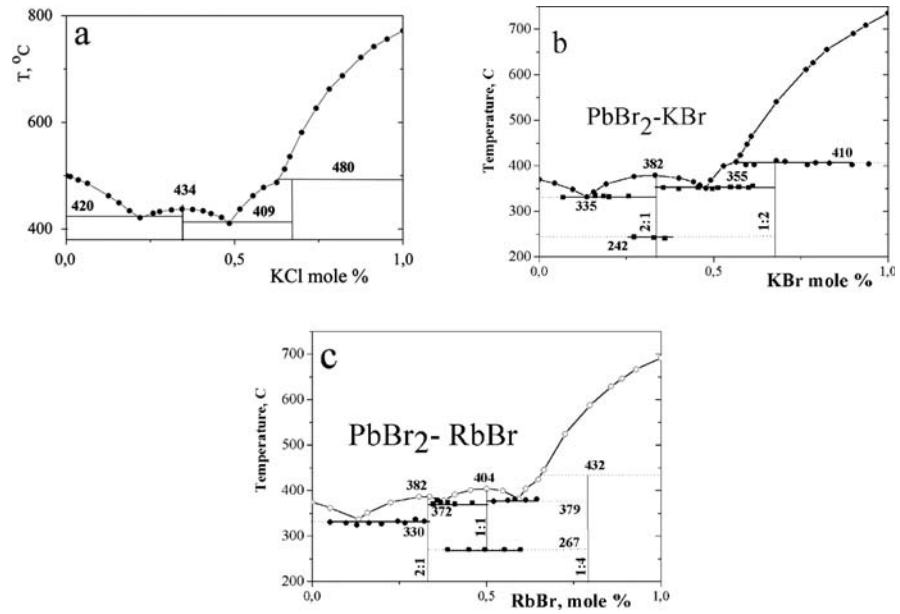

Figure 1. Phase diagrams for KCl-$PbCl_2$ (a), KBr-$PbBr_2$ (b) and RbBr-$PbBr_2$ (c) [49, 52].

of ampoule translation into cold zone was 2 to 4 mm/day. We found regimes for obtaining single crystals of both undoped and RE-doped MPb_2Hal_5 compounds with M = K, Rb, Hal = Cl, and Br, of optical quality and with sizes ∼15 mm in diameter and up to 40 mm long.

Generally, halides such as chlorides and bromides hydrolyse and therefore crystals contain some products of hydrolysis. The most frequent radicals in MHal are anions like $(OH)^-$, $(O_2)^-$, and $(CO_2)^{2-}$ [51]. When heated, $PbHal_2$ not only hydrolyses but also decomposes. Moreover, if the material contains water molecules or other impurities, decomposition increases. Because RE-doped halides as well as the halide components of MPb_2Hal_5 are sensitive to oxygen and moisture, it is imperative that both O_2 and H_2O be strictly excluded from the system. The best results are obtained when both $PbHal_2$ and MHal were dried in a vacuum and treated afterwards in Ar-$CHal_4$ atmosphere. It is important also to prevent any contact between purified material and air (i.e. oxygen and water) in both the handling operations of starting materials and the single-crystal growth process.

Segregation coefficient, K, for halide crystals (where K is the ratio of RE concentration in crystal to RE concentration in melt for specific RE dopant), was determined by both crystal type and RE ion type: it varies from 0.1 to 1 (*Figure* 2). The segregation coefficient depends considerably on the difference between sizes of RE and Pb ions. It is minimal for small Yb ions and reaches unity for large Nd ions. Growth conditions for obtaining high quality crystals depend strongly on existence of phase transitions in the solid below melting temperature. Such

TABLE 2. Experimental and calculated frequencies of Raman-active lattice vibrational modes in KPC crystals [66].

A_g, $\omega(cm^{-1})$		B_g, $\omega(cm^{-1})$	
Calculation	Experiment	Calculation	Experiment
33.4 i		37.7*i*	
16.5 i		28.3*i*	
7.7 i		6.2	
16.7	18	28.0	33
35.0	27	38.3	40
39.6	35	43.9	42
43.7	43	46.1	48
43.7		46.1	
51.9	50	57.0	57
56.5	56	65.0	
57.7		68.6	
61.8	62	72.2	75
70.1	73	74.1	
73.9		81.9	85
77.6		84.7	
86.7	85	89.1	88
88.7		95.7	95
93.1		100.7	
101.7		102.7	108
103.2	108	105.0	119
112.7	120	115.0	132
124.5	124	120.7	144
127.1	127	128.4	158
132.6	132	137.9	173
158.3	200	161.7	202

projection operators [65]. The experimental and calculated frequencies of the Raman spectrum are given in TABLE 2.

Note that these experimental and calculated frequencies agree well in the middle portion of the spectrum. For the lowest frequencies (below 20 cm^{-1}), the calculated frequencies depend strongly on small changes in the atomic coordinates; their variation within the experimental error can result in significant (up to 100 %) changes in the vibration frequencies. A large number of vibrations in this portion show weak lattice stability: it is likely a result of a near phase transition.

A larger discrepancy at high frequencies (the understated calculated values) may be due to an incomplete consideration of the shape of electronic cloud of weakly polarized Cl ions in frames of multipole approximation (a partial covalence of M-Cl bonds). One can see that position of the peak with maximal frequency depends considerably on the halogen type (*Figure* 8): thus halogen ions take part in this vibration.

2.4.3. *Absorption and reflection spectra*

Absorption spectra for MPb_2Hal_5 crystals are shown in *Figure* 9, both in the IR (*Figure* 9a) and UV-visible region (*Figure* 9b). Position of the long-wave edge of the transparency range is determined by masses of the participating ions and vibration frequencies. It is 20 μm(500 cm^{-1}) for KPC and 32 μm (312 cm^{-1}) for KPB, as estimated on the 1 cm^{-1} absorption level. Taking into account that $h\omega_{max} < 250\,cm^{-1}$ and $< 150\,cm^{-1}$ from Raman spectroscopy, one can conclude that long-wave transparency edge is determined by two-phonon absorption. The short-wave edge of the transparency range was determined as a result of approximation of the fragments with maximal inclination angle relative to the abscissa in *Figure* 9 b until crossing with this axis (TABLE 3). Chlorides demonstrate maximum of transparency at short waves (RPC is transparent up to 306 nm), whereas for bromides the edge is shifted to longer waves (∼400 nm). The absorption edge shifts to lower energies when temperature increases. Analysis of the reflection spectra reveals several dips at shorter wavelengths, which are better pronounced at temperatures as low as 8 K (*Figure* 10). These dips are related to exciton absorption and their position depends on M and Hal components and on temperature. The average temperature coefficient for the main peak E_1 in the 8 to 290 K range is $\partial E_1/\partial T = -(2.8\text{–}3.0) \times 10^{-4}$ eV/K. These values as well as specific form of the reflection spectra are typical of large radius excitons. Analysis of exciton peak positions carried out in frames of hydrogen-like Wannier-Mott model [67] allowed one to determine the band gap value E_g and exciton bonding energy R

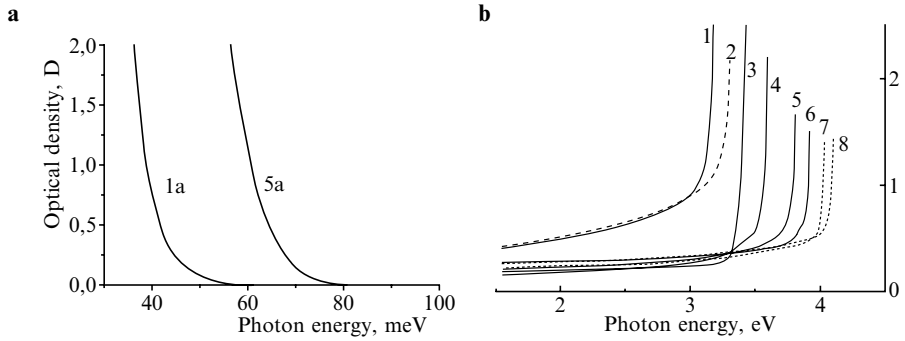

Figure 9. Absorption spectra for undoped crystals KPB (1, 1a, 2), RPB (3, 4), KPC (5, 5a, 7) and RPC (6, 8), recorded at 290 K (1, 1a, 3, 5, 5a, 6) and 8 K (2, 4, 7, 8).

TABLE 3. Position of the short-wave absorption edge at 300 K and 8 K, band gap E_g from reflection spectra (8 K) and exciton parameters E_1, R (8 K) for different halide crystals.

Parameter	Short-wave absorption edge				E_g, eV	E_1, eV	R, eV
Temperature	300 K		8 K				
	E, eV	λ, nm	E, eV	λ, nm			
KPb_2Cl_5	3.77	329	3.99	310	4.79	4.45	0.34
KPb_2Br_5	3.10	400	3.23	383	4.12	3.87	0.25
$RbPb_2Cl_5$	3.89	318	4.06	306	4.83	4.51	0.34
$RbPb_2Br_5$	3.36	370	3.56	348	4.22	4.0	0.22

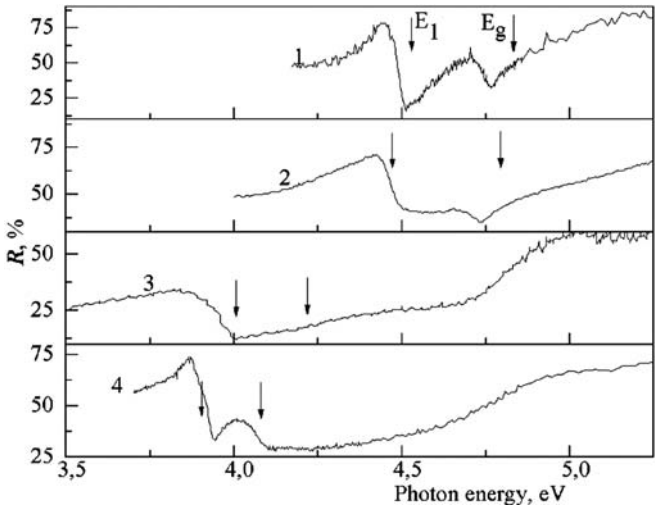

Figure 10. Fragments of reflection spectra for RPC (1), KPC (2), RPB (3) and KPB (4), recorded at 8 K. Arrows show position of the first exciton peak E_1 and band gap E_g.

(TABLE 3). Crystal RPC has maximal band gap and the E_g value decreases when Cl is replaced with Br. As follows from TABLE 3, the real short-wave absorption edge is located in MPb_2Hal_5 crystals at longer wavelengths relative to E_g position: thus it is due to excitonic absorption.

2.4.4. *Photoluminescence and luminescence excitation spectra*

In the photoluminescence (PL) spectra of MPb_2Hal_5 crystals one can see broad non-elementary bands in 1.6–2.9 eV region, with their shape and maximal position depending on M and Hal components as well as on excitation wavelength. In *Figure* 11, PL spectra for RPC (a) and RPB (b) at different excitations are

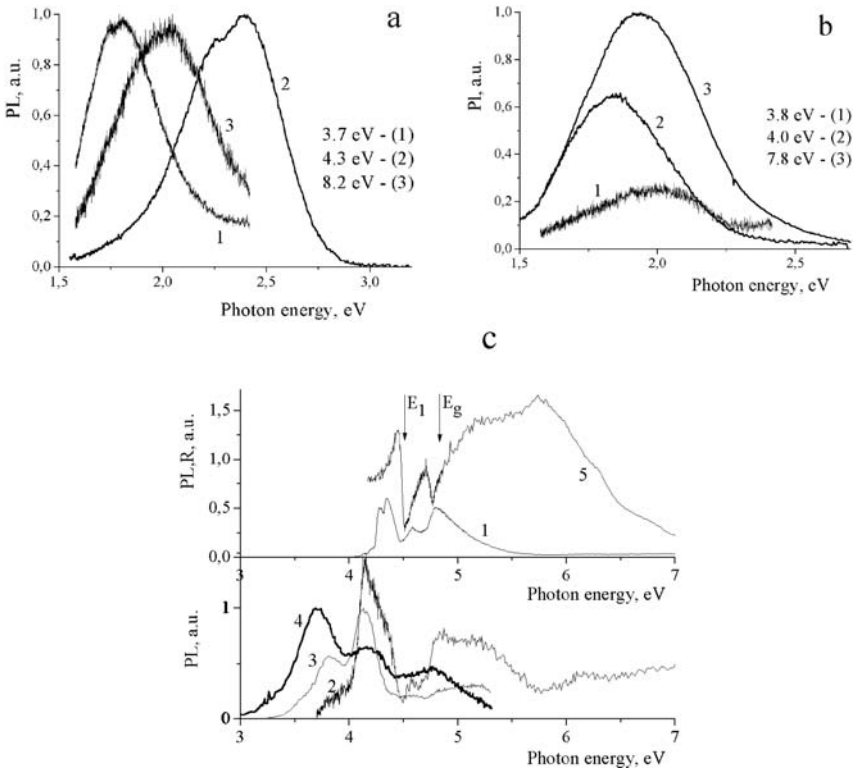

Figure 11. Low temperature photoluminescence spectra (a, b) and luminescence excitation spectra (c). Photoluminescence spectra recorded at 8 K for RPC (a) and RPB (b) at different excitation: in the transparency region (1), in exciton absorption range (2) and in the range of band-to-band electronic transitions (3). c) Luminescence excitation spectra for RPC (1–4) for 2.4 eV (1) and 2.0 eV PL(2–4) in comparison with the reflection spectrum (5). Spectra (1, 2, and 5) were recorded at 8 K whereas (3, 4) were obtained at 80 and 300 K, respectively.

given. In the general case, one can see that different PL bands are excited in the transparency region, in exciton absorption range and in the range of band-to-band electronic transitions (*Figure* 11 a), although their position is sometimes close (for example, for bromides (*Figure* 11 b)). For RPC, the short-wave PL with maxima at 2.0 and 2.4 eV takes place only at band-to-band or excitonic excitations as well as in the region of inter-band transitions whereas a long-wave PL component ($\sim$1.75 eV) corresponds to intra-center transitions in the defects. Intensity of 2.0–2.4 eV PL is maximal at low temperatures of 8–50 K and decreases as temperature increases: PL becomes completely quenched at $\sim$200 K. The luminescence excitation spectra (LES) demonstrate a set of bands depending on the crystal type: those for RPC are given in *Figure* 11 c.

In all cases, PL intensity decreases in region of inter-band transitions, at excitation energies $h\nu > E_g$, and the antibate behaviour of details takes place between

reflection and luminescence excitation spectra (*Figure* 11 c). Specific features are considered in the region of E_g and excitonic absorption maxima. The LES long-wave edge for 2.0–2.4 eV PL coincides with a long-wave edge of the transparency spectrum (*Figure* 9 b). In the case of excitation in the transparency range, excitation efficiency increases as temperature increases to 80 and 300 K (*Figure* 11 c, spectra 2–4), which can testify to thermally activated processes with participation of native or impurity defects.

2.4.5. *Electronic excitations and energy transfer*

Comparison of the obtained experimental results on spectroscopy of MPb_2Hal_5 crystals with known data concerning $PbHal_2$ testifies to similarity of these crystal families from the point of view of physics of low-energy electronic excitations and dominating input of lead cations into formation of electronic structure of the states, which determine electronic transitions with minimum energies.

In $PbHal_2$ the valence band top is formed by hybridizated orbitals of $6s$ states of Pb^{2+} and np-states of Hal^- ions ($n = 4$ for Hal = Br and $n = 3$ for Hal = Cl). Below, there are orbitals formed by np-states of Hal^- ions [68]. Since bottom of the $PbHal_2$ conduction band is formed mainly by $6p$ orbitals of Pb^{2+} ion, electronic transitions with minimum energy take place between Pb ion states and correspond to $6s \rightarrow 6p$ electric dipole transition, bringing to excitation the cation exciton [69–71].

Thus, features in low-temperature reflection spectra of MPb_2Hal_5 crystals may be related to electric dipole transitions $6s \rightarrow 6p$ between Pb^{2+} states, bringing about cation exciton excitation. Analysis of exciton parameters (TABLE 3) [69–72], calculated in frames of hydrogen-like model, allows one to suppose that observed excitonic-related features in reflection spectra (*Figure* 10) correspond to first (E_1) and second excited states of free large-radius exciton. Typical dissociation channels for such exciton may be vibrational relaxation with further radiative annihilation, energy transfer to impurity or native defects with further PL in such center, non-radiative recombination in surface states and, finally, dissociation into individual charge carriers or partly bonded electron and hole pairs.

Radiative exciton dissociation usually results in a set of specific narrow PL bands near the fundamental absorption edge. Such near-edge PL was not found for MPb_2Hal_5 crystals but several bands in low-temperature PL spectra are obviously of excitonic origin. Among them are a short-wave 3.65 eV band in KPC and a weak 2.9 eV band in KPB, which are observed only at low temperatures and are not associated with any defect. There are exponential components in decay kinetics and these bands are excited only near the fundamental absorption edge. Considerable Stokes shift (0.4–0.5 eV) and large width of PL bands mean that excitonic emission appears after vibrational relaxation and therefore the exciton undergoes self-trapping. At 8 K, the mentioned PL bands appear only at excitation

in low-energy excitonic absorption band, which corresponds to $6s^2 \rightarrow 6s6p$ transition in Pb^{2+} ion. Further increase of photon energy results in a fast decline of PL excitation efficiency because of increasing input of non-radiative losses. It is an evidence of high mobility of excitons photo-excited in the excitonic band. Excitation of short-wave PL in the range of interband transitions ($h\nu > E_g$) is of low enough efficiency and it shows a low efficiency of recombination channel for these PL bands. Indeed the 3.65 eV band was not found in either X-ray excited or thermo-activated luminescence.

Incorporation of the RE ions such as Pr, Er, Nd, Ho, Tb, and Tm results in the appearance of typical PL emission with a well-pronounced fine structure: a set of lines and relative intensity depend considerably on the RE type [72]. Impurity emission appears both at a selective direct excitation of the impurity (RE) center by photons with $E_{exc} < E_g$ energy and at indirect excitation by high energy photons with $E_{exc} \geq E_g$. In the first case, the lines in LES spectra characterize position of the excited states in energy diagram of the impurity center.

Concerning high energy excitation, the analysis of spectra shows an effective energy transfer both by excitonic mechanism and as a result of migration of free electrons and holes with their further recombination in the RE ion. The energy transfer efficiency depends on temperature: it is higher at low temperatures. On the other hand, at $E_{exc} > E_g$ the efficiency decreases as photon energy increases, which is due to growth of kinetic energy of created charge carriers and their non-radiative annihilation on crystal surface. A multiplication effect is absent for electronic excitations for energies, $E_{exc} > (2-3)E_g$, and this fact confirms efficiency of the surface losses channel. At $T = 8\,K$ there is low probability of exciton thermal dissociation in KPC crystals: thus excitonic mechanisms of energy transfer are effective. Analysis of optical spectroscopy data for KPC with Ho or Er as dopants shows that one of the possible mechanisms of RE excitation at low temperatures is a non-radiative resonant transfer of self-trapped exciton (STE) to impurity center as a result of the dipole-dipole interaction. In fact, there are several broad overlapping PL bands centered at 2.4 and 1.9 eV with microsecond decay and a fast emission at 3.75 eV with $\tau_1 = 0.8$ nsec, $\tau_2 = 3.5$ nsec. The 1.9 eV emission is due to crystal lattice defects in KPC, whereas 2.4 and 3.75 eV bands correspond to radiative annihilation of triplet and singlet self-trapped excitons, respectively. At room temperature, the STE emission is thermally quenched. Moreover, a thermal dissociation of non-relaxed excitons is possible. In such conditions, an electron-hole mechanism of energy transfer is dominating and recombination luminescence of the impurity (RE) center is observed.

2.5. KEY PHYSICAL PROPERTIES

The MPb_2Hal_5 crystal-hosts are of high transparency in the UV to mid-IR spectral range (from 0.3 to 30 μm), have satisfactory mechanical properties, high

TABLE 4. The main physical properties of MPb_2Hal_5 crystals.

Property	KPC	RPC	KPB	RPB
Transparency range, μm	0,33–20	0,32–20	0,4 −30	0,37 −30
Space group	$P2_1/c - C_{2h}^5$	$P2_1/c - C_{2h}^5$	$P2_1/c - C_{2h}^5$	$I4/\mathrm{mcm} - D_{4h}^{18}$
Melting temperature, °C	434	423	382	382
Density, g/cm^3	4,629	5.041	5,619	5.83
Refraction index at 300 K	$n_x = 1.9406$ $n_y = 1.9466$ $n_z = 1.9724$ (at 1 μ m)	$n = 2,019$ (at 0.63 μm)	$n_x = 2,191$ $n_y = 2,189$ $n_z = 2,247$ (at 0.63 μm)	$n_o = 2,2410$ $n_e = 1,9654$ (at 0.63 μm)
Thermo-optic coefficient $\beta^*(10^{-5})$, $°C^{-1}$ (near 300 K)	−7.0 −10.0 −10.5 (at 1 μm)		−13.0 −14.1 −14.9 (at 1 μm)	
Thermal conductivity, W/m*K	4	4		
Mohs hardness	2,5	2,5	2,5	2,5
Maximal phonon energy, $\hbar\omega_0$, cm^{-1}	203	203	138	138
Chemical stability	stable	stable	stable	stable

chemical resistance, low hygroscopicity, extremely low maximal phonon energy ($\sim$200 cm^{-1} in chlorides and $\sim$150 cm^{-1} in bromides), and incorporate RE^{3+} ions with concentration up to 3%. The main physical properties of MPb_2Hal_5 crystals are summarized in TABLE 4.

3. Spectroscopic characteristics of RE^{3+} ions in MPb_2Hal_5 crystals

Up to now, the strategy used to search for new laser channels of RE^{3+} activated crystals involves the problem of determining their spectroscopic characteristics. The feasibility of exciting stimulated emission on f-f transitions of RE^{3+} ions is most often reduced to the estimate of luminescence quantum yield for steady-state excitation. From the 1970's until now comparatively simple semi-empirical methods for determination of the most important intensity characteristics of

Acknowledgments

It is a pleasure to acknowledge Prof. W. Krupke for initialization of this work and Prof. S. Payne of Lawrence Livermore National Laboratory for his support through CRDF Grant No. RE2 2222. We would like to thank Dr. M.-F. Joubert and Dr. Y. Guyot for fruitful discussions and kind help with kinetics experiments. We acknowledge Profs.V.A. Pustovatov and I.N. Ogorodnikov for the VUV spectroscopic measurements, Prof. A.N. Vtyrin and Drs. S.V. Melnikova, A.A. Merkulov for study of phase transitions and Dr. V.P. Gapontsev for help with LD pumping sources.

The authors from State Optical Institute acknowledge the support of INTAS, grant No. INTAS-97-787 and Russian Foundation for Basic Researches, grants No. 00-02-16637 and 03-02-17196.

References

1. A.A. Kaminskii, in *Crystalline Lasers:Physical Processes and Operating Schemes*, (CRC Press N.Y. London, Tokyo, 1996).
2. S.A. Pollack, D.B. Chang, *J. Appl. Phys.* **64**(6), 2885–2893 (1988).
3. F. Auzel, S. Hubert, D. Meichenin, *Appl. Phys. Lett.* **54**(8), 681–683 (1989).
4. M. Pollnau, R. Spring, S.Wittwer, W. Luthy, H.P. Weber, *J. Opt. Soc. Am.B* **14**(4), 974–978 (1997).
5. A. Shmaul, G. Huber, R. Clausen, B. Chai, P. LiKamWa, M. Bass, *Appl. Phys. Lett*. **62**(6), 541–543 (1993).
6. R.S. Stoneman, J.G. Lynn, L. Esterowitz, *IEEE Journal of Quantum Electronics* **28**(4), 1041–1045 (1992).
7. T. Jensen, A. Diening, G. Huber, B.H.T. Chai, *Optics Letters*, **21**(8), 585–587 (1996).
8. M. Pollnau, R. Spring, Ch. Ghisler, S. Wittwer, W. Luthy, H.P. Weber, *IEEE Journal of Quantum Electronics*, **32**(4), 657–662 (1996).
9. Chr. Wyss, W. Luthy, Heinz P. Weber, *IEEE Journal of Quantum Electronics* **34**(6), 1041–1045 (1998).
10. G.R. Knitz, R. Allen, L. Esterowitz, *Appl. Phys. Lett.* **50**(22), 1553–1555 (1987).
11. S. Hubert, D. Meichenin, F. Auzel, *Journal of Luminescence* **45**, 434–436 (1990).
12. Chr. P. Wyss, W. Luthy, H. P. Weber, L. Brovelli, Ch. Harder, H. P. Meier, P. Rogin, J. Hulliger, *Proceedings of Biomedical Systems and technologies II, SPIE Proceedings series* **3199**, 206–213 (1997).
13. V.V. Shumilin, A.M. Tkachuk, V.V. Laso, N.N. Smirnov, V.F. Danilichev, A.F. Gatzu, D.V. Ganin, *Proceedings of 4^{th} International Conference on Laser Applications in Life Sciences, 7–11 September, 1992, Juvaskyla, Finland,* 255–262 (1992).
14. A. Diening, G. Huber, *Book of Abstracts of Conference on Lasers and Electrooptics CLEO 2000*, CFA3 (2000).

15. Chr. P. Wyss, W. Luthy, H.P. Weber, P. Rogin, J. Hulliger, *Optical Communications* **139**, 215–218 (1997).

16. S.A. Pollack, D.B. Chang, R.A. MacFarlane, H. Jenssen, *J. Appl. Phys.* **67**(2), 648–653 (1990).

17. M. Pollnau, W. Luthy, H.P. Weber, T. Jensen, G. Huber, A. Cassanho, H.P. Jenssen, R.A. MacFarlane, *Optics Letters* **21**(1), 48–50 (1996).

18. C.S. Knowles, H.P. Jenssen, *IEEE Journal of Quantum Electronics* **28**(4), 1197–1208 (1992).

19. A.A. Kaminskii, S.E. Sarkisov, F. Belov, H.-J. Eichler, *Optical and Quantum Electronics* **22**, S95–S105 (1990).

20. A.M. Tkachuk, S.E. Ivanova, M.-F. Joubert, Y.Guyot, and V.P. Gapontzev, Population of Excited Erbium Levels in Er^{3+}:$Na_{0.4}Y_{0.6}F_{2.2}$ (Er:NYF) Laser Crystals, *J. Alloys and Comp.* **380**(1–2) 130–135 (2004).

21. B.M. Antipenko, B.V. Sinitzin, T.V. Uvarova, *Kvantyovaya electronika* **7**, 2019–2022 (1980).

22. G.D. Gilliland, R.C. Powell, L. Esterowitz, in *Dig. Topical Meeting on Tunable Solid State Lasers, Williamsburg, Virginia, 1987,* WE4, (1987).

23. B.M. Antipenko, I.G. Podkolzina, Yu. V. Tomashevitch, *Kvantyovaya electronika* **7**, 647–649 (1980).

24. N. Djeu, V.E. Hartwell, A.A. Kaminskii, A.V. Butashin, *Optics Letters* **22**(13), 997–999 (1997).

25. L.F. Johnson, H.J. Guggenheim, *Appl. Phys. Lett.* **23**, 96 (1973).

26. B.M. Antipenko, A.L. Ashkalunin, A.A. Mak, B.V. Sinitzin, Yu. V. Tomashevitch, G.S. Shahkilimyan, *Kvantyovaya electronika* **7**(5), 983–987 (1980).

27. N.P. Barnes, L. Esterowitz, R. Allen, *in Tech. Digest Papers Conf. Lasers and Electro-Optics* (*OSA, Washington, D.,C., 1984*), WA5 (1984).

28. R.C. Eckardt, L. Esterowitz, I.D. Abella, *in Digest Tech. Pap. Conf. Lasers and Electro-Optics* (*OSA/IEEE, Washington, D.,C., 1982*), 160 (1982).

29. L. Esterowitz, R.C. Eckardt, R.E. Allen, in *Digest Tech. Pap. Conf. Lasers and Electro-Optics* (*OSA/IEEE, Washington, D.,C., 1982*), 160 (1982).

30. A.A. Kaminskii, K. Kurbanov, T.V. Uvarova, *Izv. Akad. Nauk SSSR Neorg. Mater.* **23**, 1049 (1987).

31. R.H. Page, K.I. Schaffers, S.A. Payne, W.F. Krupke, Dy-Doped Chlorides as Gain Media for 1.3 mm Telecommunications Amplifiers, *J. Lightwave Technol.* **15**(5), 786–793 (1997).

32. L.I. Isaenko, A.P. Yelisseyev, V.A. Nadolinny, V.I. Pashkov, M.C. Nostrand, S.A. Payne, R.H. Page, and R.W. Solarz, Growth and Spectroscopic Properties of Rare Earth doped Chloride Crystals for Telecommunication Amplifiers, in *Solid State Lasers VII, R. Scheps, ed, Proc. SPIE* **3265**, 242–249 (1998).

33. M.C. Nostrand, R.H. Page, S.A. Payne, W.F.Krupke, P.G. Schunemann, and L.I. Isaenko, Spectroscopic data for infrared transitions in $CaGa_2S_4$:Dy^{3+} and KPb_2Cl_5:Dy^{3+}, in *Advanced Solid State Lasers, W.R. Bosenberg and M.M. Fejer, ed., OSA TOPS*. **19,** 524–528 (1998).

34. Alexandra Tkachuk, Svetlana Ivanova, Ludmila Isaenko, Aleksandr Yelisseyev, Stephen Payne, Richard Solarz, Mike Nostrand, Ralph Page, Comparative Spectroscopic Study of the Dy^{3+} Doped Double Chloride and Double Fluoride Crystals for Telecommunication Amplifiers and IR Lasers, *Acta Physika Polonika A* **95**(3), 381–394 (1999).

35. A.M. Tkachuk, S.E. Ivanova, L.I. Isaenko, A.P. Eliseev, W. Krupke, S. Payne, R. Solarz, M. Nostrand, R. Page, and Stephen Payne, Dy^{3+} doped crystals of double chlorides and double fluorides as the active media of IR solid-state lasers and telecommunication amplifiers, *J. Optical Technology* **66**(5), 460–462 (1999).

36. M.C. Nostrand, R.H. Page, S.A. Payne, and W.F. Krupke, P.G. Schunemann, Room-temperature laser action at 4.3–4.4 μm in $CaGa_2S_4$:Dy^{3+}, *Opt. Lett*. **24**(17), 1215–1217 (1999).

37. M.C. Nostrand, R.H. Page, S.A. Payne, W.F. Krupke, P.G. Schunemann, L.I. Isaenko, Room temperature $CaGa_2S_4$:Dy^{3+} laser action at 2.43 and 4.31 μm and KPb_2Cl_5:Dy^{3+} laser action at 2.43 μm, *OSA TOPS in Optics and Photonics Series*, *ASSL*, **26**, 441–449 (1999).

38. M.C. Nostrand, R.H. Page, S.A. Payne, W.F. Krupke, P.G. Schunemann, L.I. Isaenko, Laser Demonstrations of Rare-Earth Ions in Low-Phonon Chloride and Sulfide Crystals, *OSA TOPS in Optics and Photonics Series, ASSL,* **34**, 459–463 (2000).

39. M.C. Nostrand, R.H. Page, S.A. Payne, W.F. Krupke, and L.I. Isaenko, Quantum efficiency measurements for long-wavelength operation of rare-earth doped KPb_2Cl_5, in *Technical Digest of conference on Lasers and Electro-Optics CLEO 2000, May 7–12, San Francisco, USA*, 566–56 (2000).

40. L. Isaenko, A. Yelisseyev, A. Tkachuk, S. Ivanova, S. Vatnik, A. Merkulov, S. Payne, R. Page, M. Nostrand, New laser crystals based on KPb_2Cl_5 for IR region, *Material Science and Engineering* **B81**, 188–190, (2001).

41. T.T. Basiev, M.E. Doroshenko, V.V. Osiko, D.V. Badikov, Mid-IR Laser Oscillation in new low phonon $PbGa_2S_4$:Dy^{3+} crystal, *OSA Topical Meeting, Advance Solid State Photonics, 2005*, paper TuB10, (2005).

42. S.R. Bowman, L.B. Shaw, B.J. Feldman, J. Ganem, A 7-μm Praseodymium-Based Solid-State Laser, *IEEE J. Quantum Electron*. **32**(4) 646–649 (1996).

43. K. Nitsch, A. Cihlár, Z. Málková, M. Rodová and M. Vanecek, *J. of Crystal Growth* **131** (3–4), 612–615 (1993); K. Nitsch, M. Dusek, M. Nikl, K. Pollak, and M. Rodova, Ternary alkali lead chlorides: crystal growth, crystal structure, absorption and emission properties, *Prog. Cryst. Growth Charact*. **30**, 1–22 (1995).

44. S.R. Bowman, S.K. Searles, Josef Ganem, Paul Schmidt, Further investigation of potential 4 μm materials, *OSA TOPS* **26**, *Advance Solid-State Lasers*, 487–490 (1999).

45. S.R. Bowman, S.K. Searles, N.W. Jenkins, S.B. Qadri, E.F. Skelton, Josef Ganem, New Mid-IR Laser on an Erbium activated low phonon energy crystal, *Technical Digest of conference of Lasers and Electro-Optics 2001, May 8–10, Baltimore, Maryland, USA, CLEO (2001)*, CFD2, 557–558 (2001).

46. J.L. Doualan, R. Moncorge, Laser crystals with low phonon frequencies, *Ann. Chim. Sci. Mat.* **28**, 5–20 (2003).

47. K. Nitsch, V. Hamplova, M. Nikl, K. Polak, V. Rodova, Lead bromide and ternary alkali lead bromide single crystals-growth and emission properties, *Chem. Phys. Lett.* **258,** 518–522 (1996).

48. Katja Rademaker, Ernst Heumann, Günter Huber, Stephen A. Payne, William F. Krupke, Ludmila I. Isaenko, Arnold Burger, Laser activity at 1.18, 1.07, and 0.97 mm in the low-phonon-energy hosts KPb_2Br_5 and $RbPb_2Br_5$ doped with Nd^{3+}, *Opt. Lett.* **30**(7), 729–731 (2005).

49. M. Cola, V. Massariti, R. Richard, C. Siristri, Binary systems formed by lead bromide with (Li, Na,K,Rb and Tl): a DTA and diffractometry study, *Z.Natuforsch.,* **A26**, 1328–1332 (1971).

50. M.C. Nostrand, R.H. Page, S.A. Payne, L.I. Isaenko, and A.P. Yelisseyev. "Optical properties of Dy^{3+} and Nd^{3+}– doped KPb_2Cl_5". *J. Opt. Soc. Am. B*, **18**, 264–275 (2001).
51. M. Voda, M. Al-Saleh, G. Lobera, R. Balda, J. Fernandez, Crystal growth of RE-doped ternary potassium lead chloride single crystals by the Bridgman method, *Opt. Mater*. **26**(4) 359–364 (2004).
52. A. Gabriel, A.D. Pelton, Phase diagram measurements and thermodynamic analysis of the $PbCl_2$–NaCl, $PbCl_2$–KCl and $PbCl_2$–KCl–NaCl systems, *Can.J.Chem.*, **63**, 3276–3282 (1985).
53. S.V. Melnikova, L.I. Isaenko, V.M. Pashkov, V.M. Pevnev, Study of phase transition in KPb_2Cl_5 crystal, *Fizika Tverd.Tela* **47** (2) 319–325 (2005) in Russian.
54. S.V. Melnikova, L.I. Isaenko, V.M. Pashkov, V.M. Pevnev, Search for phase transitions in some representatives of the APb_2X_5 family, *Fizika Tverd.Tela*, in press, (2006), in Russian.
55. Y.P. Beck, G. Clicque, H. Nau, A study of AB_2X_5 compounds (A:K,In,Tl; B: Sr,Sn,Pb; X: Cl,Br,I), *Z. Anorg. Allg. Chem.* **536**, 35–44 (1986).
56. H. Keller, Notiz zur Kristallstruktur von APb_2Cl_5-Verbindungen, *Z.Naturforsch*., **B31**, 885 (1976).
57. F. Ras, D. Ijdo, G.C. Verschoor, Ammonium dilead chloride, *Acta Crystallogr.*, **B33**, 259–260 (1977).
58. M. Nikl, K. Nitsch, I. Velicka, J. Hybler, K. Polak, T. Fabian, Photoluminescence of KPb_2Cl_5, *Phys.Stat.Sol.(b),* **168**, K37 (1991).
59. A. Merkulov, L.I. Isaenko, V.M. Pashkov, V.G. Mazur, A.V. Virovets, D.Yu. Naumov, Investigation of KPb_2Cl_5 and KPb_2Br_5 crystal structure, *Zhurn.Strukt.Khimii,* **6**(1) 106–110 (2005), in Russian.
60. O.V. Ivanov, D.A. Shport. E.G. Maksimov, Microscopic calculations of ferroelectric instability in perovskite crystals, *J. Exp. Theor. Physics,* **87**, 186–199 (1998).
61. N.G. Zamkova, V.I. Zinenko, O.V. Ivanov, E.G. Maksimov, S.N. Sofronova, Lattice dynamics calculations of the ionic crystals with ion dipole and quadrupole deformations: perovskite structure oxides, *Ferroelectrics,* **283**, 49–60 (2003).
62. A.N. Vtyurin, S.V. Goryainov, N.G. Zamkova, V.I. Zinenko, A.S. Krylov, S.N. Krylova, A.D. Shefer, Hydrostatic pressure-induced phase transitions in $RbMnCl_3$: Raman spectra and lattice dynamics, *Physics of Solid State*, **46**, 1301–1310 (2004).
63. M. Born and K. Huang, *Dynamical Theory of Crystal Lattices* (Clarendon, Oxford, 1954).
64. M.B. Smirnov, in: *Dynamic Theory and Physical Properties of Crystals*, edited by A.N. Lazarev (Nauka, St.Petersburg, 1992), pp. 41 (in Russian).
65. H. Streitwolf, *Gruppen theorie in der Festkoperphysik* (Teubner, Leipzig, 1967).
66. K.S. Alexandrov, A.N. Vtyurin, A.P. Eliseev, N.G. Zamkova, L.I. Isaenko, S.N. Krylova, V.M. Pashkov, P.P. Turchin, A.P. Shebanin, Vibrational spectrum ans elastic properties of the KPb_2Cl_5 crystals, *Fizika Tverd.Tela*, **47**(3) 512–518 (2005).
67. A.K.S. Song, R.T. Williams, *Self-trapped excitons* (Berlin-Heidelberg, New-York; Springer Verlag, 1996).
68. A.F. Malisheva, V.G. Plekhanov, Investigation of optical constants of $PbCl_2$ and $PbBr_2$ in the 3.5 to 11 eV energy interval, *Optika i Spectrosckopiya*, 34 (3), 527–531 (1973), in Russian.
69. V.A. Pustovarov, I.N. Ogorodnikov, S.I. Omelkov, A.A. Smirnov and A.P. Yelisseyev, Excitons and energy transport in crystals KPb_2Cl_5 and $RbPb_2Br_5$, *Nuclear Inst. and Methods in Physics Research, A.* **543**(1) 216–220 (2005).